RESEARCH ARTICLE | JANUARY 25 2022

Effects of exercise on flow characteristics in human carotids

Xinyi He (何心怡); Xiaolei Yang (杨晓雷)

Physics of Fluids 34, 011909 (2022)
https://doi.org/10.1063/5.0078061

Physics of Fluids ARTICLE scitation.org/journal/phf

Effects of exercise on flow characteristics in human carotids

Cite as: Phys. Fluids **34**, 011909 (2022); doi: 10.1063/5.0078061
Submitted: 9 November 2021 · Accepted: 16 December 2021 ·
Published Online: 25 January 2022

View Online Export Citation CrossMark

Xinyi He (何心怡),[1,2] and Xiaolei Yang (杨晓雷)[2,3,a)]

AFFILIATIONS

[1]College of Aircraft Engineering, Nanchang Hangkong University, Nanchang 330063, China
[2]The State Key Laboratory of Nonlinear Mechanics, Institute of Mechanics, Chinese Academy of Sciences, Beijing 100190, China
[3]School of Engineering Sciences, University of Chinese Academy of Sciences, Beijing 100049, China

[a)]Author to whom correspondence should be addressed: xyang@imech.ac.cn

ABSTRACT

Carotid is one of the focal regions prone to atherosclerosis. Previous studies have shown that hemodynamics plays an important role in the initiation and formation of atherosclerosis plaques. In this work, we numerically investigate the flow patterns in two carotids with different flares and proximal curvatures under inflows from three age groups with/without exercise. The simulation results show that the effects of exercising on the carotid flow and wall shear stress are different at different time instants and for different age groups. As for the oscillatory shear index, exercise does not have significant effects. The effects of inflow waveforms on the reversed flow volume are also examined. For the carotid C1 with low flare and high proximal curvature, it is found that exercising increases and decreases the reversed flow volume for young and senior people, respectively. For middle-aged people, on the other hand, the reversed flow volume is increased and decreased in the middle of the sinus and near the bifurcation, respectively, for the carotid C1. For the carotid C2 with high flare and low curvature, on the other hand, it is found that exercising increases the reversed flow volume for all age groups. This work suggests that the effects of exercise on atherosclerosis should be evaluated by fully considering patient-specific geometries and ages.

I. INTRODUCTION

Atherosclerosis, which causes stroke and heart attack, is one of the most serious diseases threatening human health. It is a complex biophysical, biochemical, and physiological process, occurring at multiple time and space scales, which brings great challenges to the early warning, diagnosis, and prevention of atherosclerosis-related diseases. Blood flows in human's cardiovascular system,[1–4] with the Reynolds number *Re* ranging from 10^3 to 10^4 for large arteries to less than 1 for small capillaries,[5] are closely related to the initiation and formation of atherosclerosis plaques, which are found at several focal locations with curvatures and branches, such as carotid and coronary arteries.

The shear stress exerted by blood flow on the intimal layer, which is composed of endothelial cells, serves as a driving force in the formation of atherosclerosis plaques. It is commonly accepted that the disturbed flow—with low mean wall shear stress (WSS), varying shear directions and magnitudes—induces atherosclerosis, although it is still debatable whether high WSS or low WSS is the cause of atherosclerosis.[6–8] Glycocalyx, a thin layer of glycolipids, glycoproteins, and proteoglycans covering the surface of mammalian epithelial cells, plays a role as the mediator and interpreter for transmitting shear stress into cells,[9,10] and its degradation inhibits the production of nitric oxide (NO), which contributes to cardiovascular disease[11] (which is also considered as a potential for targeted drug delivery[12]). Studies showed that disturbed flows induce atherosclerosis by altering gene expression in the arterial enthothelium.[6] Factors induced by disturbed flows, which promote endothelial inflammation, include the Piezo1- and Gq/G11-mediated integrin activation,[13] Smarcd3/Bap60,[14] activation of ERK1/2/eNOS-Thr495 (extracellular signal regulated kinases1/2, endothelial nitric oxide synthase, Phospho-eNOS) inhibiting endothelial NO synthase,[15] DNA methylation,[16–18] AAV8-mediated overexpression of PCSK9 (adeno-associated-virus-8, proprotein convertase subtilisin/kexin type 9),[19] and others.[20–23] The results from a mouse model study suggested that the signaling from disturbed flows also induces systemic metabolic changes.[24] There are also other factors, which are anti-atherosclerosis, such as protease-activated receptor-1 (PAR-1),[25] PRKAA1/AMPKα1 (Protein kinase AMP-activated alpha 1)-driven glycolysis,[26] and KLK10 (allikrein Related Peptidase 10) in collaboration with HTRA1 (HtrA Serine Peptidase 1).[27] It is noted that the biological/biochemical process is

not accounted for in the computational method employed in this work, which will be considered in the future.

The vascular geometry, which affects the pattern of disturbed flows,[28–30] plays an important role in the onset and development of atherosclerosis. For the carotid artery, geometrical features, such as the diameter of the sinus bulb, bifurcation angle, proximal curvature, flare, tortuosity of the common carotid (CCA) and internal carotid (ICA) arteries, have been examined in the literature.[31] Computational studies have showed that the sinus and carina regions of the ICA are sites of plaque vulnerability.[32] Kamenskiy *et al.*[33] examined the changes of carotid artery geometry with age. Their results demonstrated that larger bulb diameters with smaller bifurcation angles are associated with carotid artery diseases. The bifurcation angles and cardiac curvatures of coronary bifurcations were examined by Chiastra *et al.*[34] It was found that the bifurcation angle influences the blood flow for both stenosed and unstenosed arteries, while the curvature radius has an effect on the initiation and intensity of the helical flow structures. In the work by Nagargoje and Gupta,[35] the effects of sinus size and locations on blood flows were examined numerically. Spanos *et al.*[36] investigated the correlation of bifurcation geometry with early carotid atherosclerosis. Associations with higher intima-media thickness in the CCA were observed for larger bulb diameter, and lower ratios of (diameter of ECA + diameter of ICA)/(diameter of CCA). Furthermore, indicators were observed to be different for the right and left carotid arteries. In the work by Yao *et al.*,[37] larger values of the area with oscillatory shear index (OSI) and large ratios of the ECA/CCA diameters are observed to be related to neointimal hyperplasia. Early atherosclerosis often behaves as positive remodeling, i.e., compensatory enlargement of the outer wall. Magnetic resonance imaging results of 525 subjects showed a large possibility of positive remodeling in the CCA, negative remodeling over the bifurcation, and mixed patterns in the ICA.[38] Studies of 501 carotid arteries with nonstenotic atherosclerosis showed that the luminal expansion FlareA is associated with vulnerable plaque.[39] In the work by Gregg *et al.*,[40] the carotid bulb inflow area and the bifurcation angle are found to be positively correlated with the plaque volume. Strecker *et al.*[41] showed that high carotid tortuosity and low ICA diameter are independent predictors for the wall thickness of the ICA bulb. Bijari *et al.*[42] showed that high flare and low proximal curvature prompt the formation of plaques. Numerical results from the study carried out by Chen *et al.*[43] showed that the length of time with reverse flows and the intensity of velocity variations are higher for carotids with high flare and low proximal curvature.

Inflow also plays a role in the dynamics of blood flow. The age and life style of individuals affect the shape of inflow waveforms. As shown in the work by Azhim *et al.*,[44] the maximum flow rate at the peak systole significantly decreases with aging. For people of similar age, exercise affects the maximum flow rate as well as the time instants when the maximum and minimum flow rates occur for the systole and diastole cycles, respectively. The study of Rauramaa *et al.*[45] showed that exercise can promote the thinning of intima-media thickness for people who are not taking statins; for other people, however, it is not clear that aerobic physical activity can slow the development of atherosclerosis. Kadoglou *et al.*[46] showed that insufficient physical activity is related to an increase in carotid intima-media thickness, and stated that the effect of long-term exercise on atherosclerosis is still unclear as in the work by Rauramaa *et al.*[45] Huang *et al.*[47] numerically examined three different inflow waveforms with different locations of the peak systole, and observed similar flow patterns including the wall shear stress at peak systole and the OSI for an idealized bifurcation

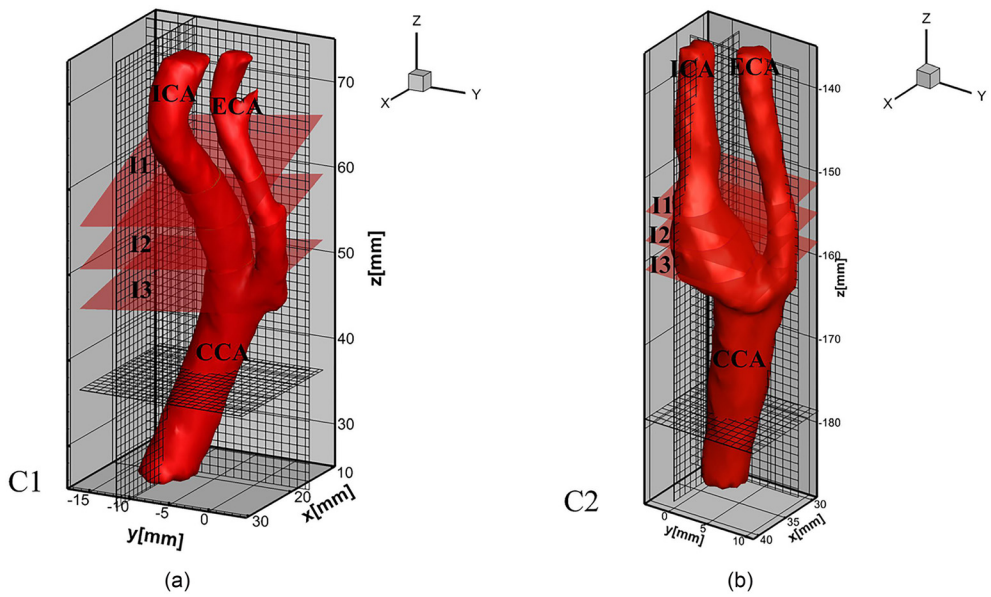

FIG. 1. Geometric image of two carotid arteries with the background Cartesian grid for blood flow simulations. CCA: common carotid artery, ICA: internal carotid artery, and ECA: external carotid artery. I1, I2, and I3 indicate the three slices at different downstream locations relative to the carotid sinus. For the background grid, every tenth grid line is displayed for clarity.

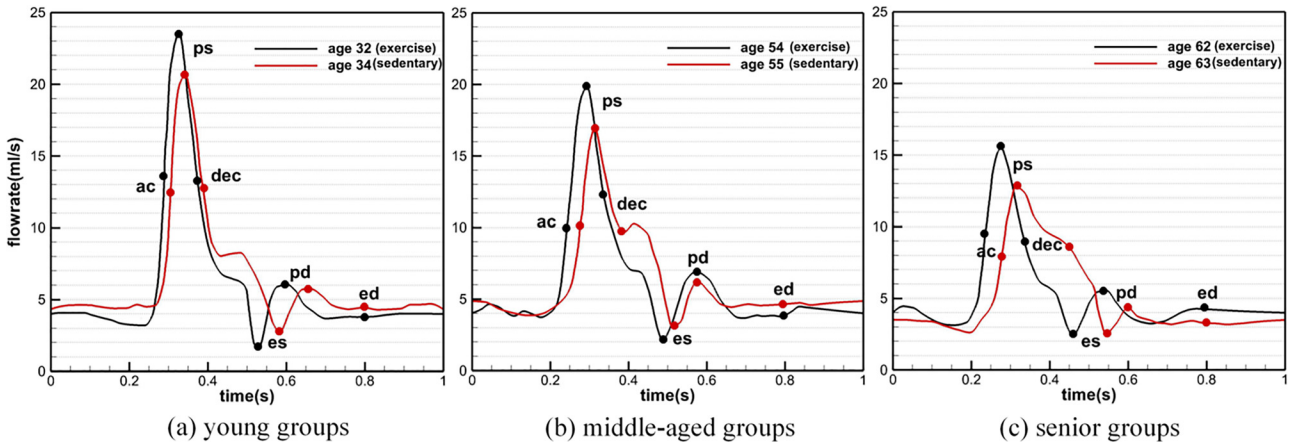

FIG. 2. Waveforms of the pulsatile flow rates applied at the inlet of the CCA of the carotid artery under different exercise conditions for (a) young, (b) middle-aged, and (c) senior groups. These inflow waveforms are digitized from the work by Azhim *et al.*[44]

model. It is still not clear how different inflow waveforms due to aging and exercise affect the flow patterns in realistic human carotids with different geometric features.

Flow patterns in different shapes of arteries have been studied in the literature. In the carotid artery under pulsatile inflow, C-shaped axial velocity patterns and Dean-type vortices are observed at the deceleration phase and at the end of the systole phase in a model carotid[48] and six different carotids from healthy human.[43] In the work by Chen *et al.*,[43] the C-shaped axial velocity pattern was further classified by considering its streamwise variations. The secondary flow

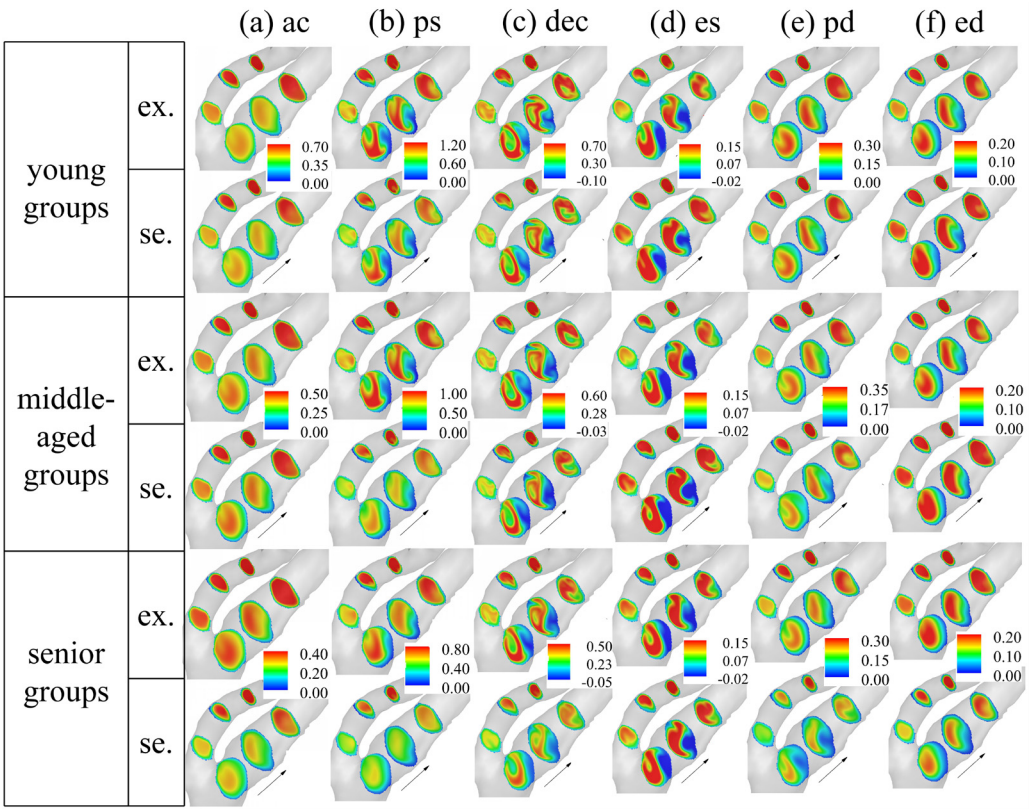

FIG. 3. Contours of the axial velocity of carotid C1 under exercise and sedentary conditions for the young, middle-aged, and senior groups, at the acceleration (a), peak systole (b), deceleration (c), end systole (d), peak diastole (e), and end diastole (f). Legend of contour: axial velocity (m/s).

induced by curvature was studied for relatively simple shapes in these papers.[49–52] The effects of carotid geometry on the secondary flow were investigated by Chen *et al.*,[43] where significantly different flow patterns were observed for different carotids and at different instants of the cardiac cycle. Buchmann and Jermy[53] argued that the location and timing of these flow structures can ultimately affect the formation of atherosclerosis plaques, although the time scale of a cardiac circle (1 s) is orders of magnitudes lower than that of the pathology of atherosclerosis (years). Gataulin *et al.*[54] simulated the blood flow in two model common carotid arteries and observed intensive swirls at the deceleration phase, which was also observed in the work of Chen *et al.* for human carotids.[43] The effects of symmetric and asymmetric bifurcation on the dynamics of pulsatile flow were investigated by Nagargoje *et al.*[29] for both Newtonian and non-Newtonian fluids. The flow patterns in arteries with stenosis were also investigated.[55,56] Song *et al.*[57] investigated the effects of symmetrical and asymmetrical stenosis on the distribution of wall shear stress for tortuous coronary arteries. Freidoonimehr *et al.*[28] found that the shape of stenosis in a coronary artery can significantly affect the length of the jet region. The effects of stenosis on flow separation and transition to turbulence were investigated by Ding *et al.*[58] for a two-dimensional channel. The effect of inflow on vortex formation and wall shear stress were investigated by Cox and Plesniak,[59] showing that the vortex and the secondary flow are less intense for the case with uniform inflow when compared with a fully developed inflow.

This work is devoted to investigate the patterns of disturbed flows in two different carotids, one with high risk geometrical factors, i.e., high flare and low proximal curvature, and the other without, for different inflow waveforms, which cannot be easily accomplished via *in vitro* or *in vivo* experiments.[60,61] Multiscale computational models have been developed in the literature[62–65] toward understanding the coupling between cell-level processes and the blood flow. In this work, however, we will focus on the blood flow at the macroscopic scale without considering the chemical and physiological process associated with gene expression at the cell level. With the above considerations and considering the size of the carotid artery, the blood is assumed to be Newtonian in this work. For the non-Newtonian characteristics of the blood, the authors can refer to the review by Beris *et al.*[66] and several other related papers,[67–69] where viscoelasticity, viscoplasticity, and the thixotropic nature of the blood are studied.

The rest of this paper is organized as follows. The employed numerical method and the case setup are introduced in Sec. II. Following the case setup, the obtained simulation results are analyzed in Sec. III. At last, conclusions are drawn in Sec. IV.

II. NUMERICAL METHODS AND CASE SETUP

A. Numerical methods

The virtual flow simulator (VFS-Wind) code,[70–73] which has been successfully applied to simulate flows over complex geometries,[74–76] is employed for simulating the flow in human carotids.

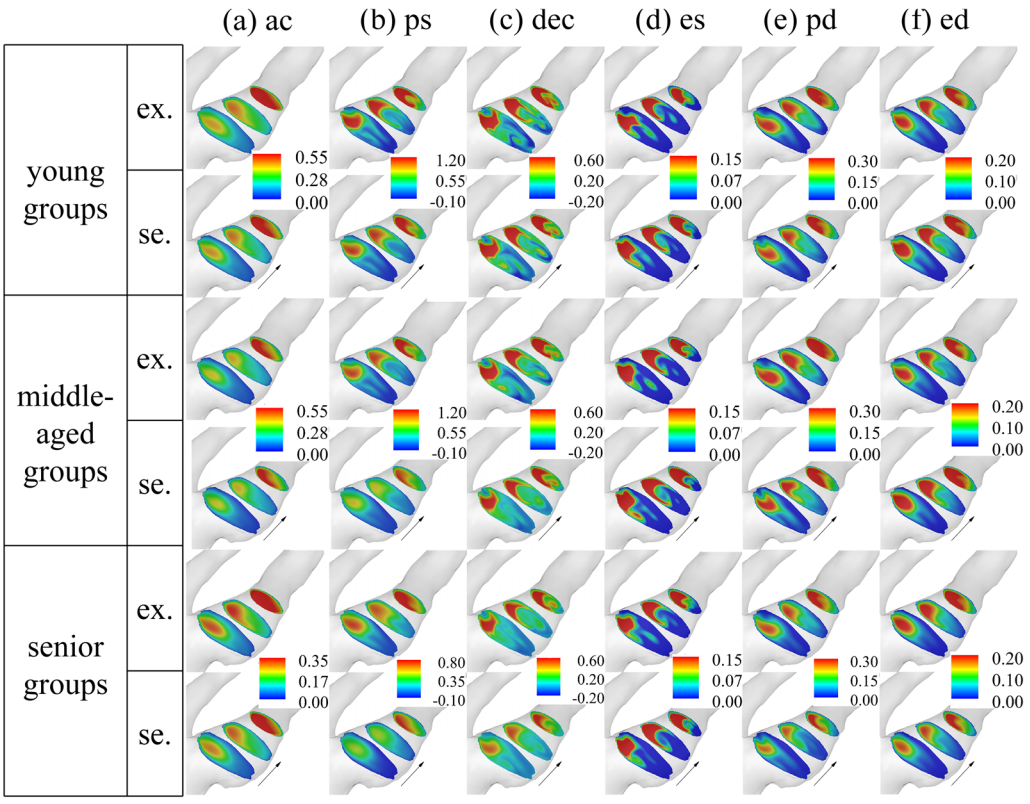

FIG. 4. Contours of the axial velocity of carotid C2 under exercise and sedentary conditions for the young, middle-aged, and senior groups, at the acceleration (a), peak systole (b), deceleration (c), end systole (d), peak diastole (e), and end diastole (f). Legend of contour: axial velocity (m/s).

The blood flow is assumed to be incompressible and Newtonian. The governing equations are the incompressible Navier–Stokes equations as follows:

$$\frac{\partial u_j}{\partial x_j} = 0, \tag{1}$$

$$\frac{\partial u_i}{\partial t} + \frac{\partial u_i u_j}{\partial x_j} = -\frac{1}{\rho}\frac{\partial p}{\partial x_i} + \nu \frac{\partial^2 u_i}{\partial x_j \partial x_j}, \tag{2}$$

where x_i ($i = 1, 2, 3$) are the Cartesian coordinates, u_i is the ith component of the velocity vector, ν is the kinematic viscosity, ρ is the density, and p is the pressure. The governing equations are discretized in space using a second-order accurate central differencing scheme, and integrated in time using the fractional step method.[77] An algebraic multigrid acceleration along with a GRMES solver is used to solve the pressure Poisson equation. A matrix-free Newton–Krylov method is used for solving the discretized momentum equations.

The curvilinear immersed boundary (CURVIB) method[77–81] is employed to model the geometry of the carotid, in which the flows are solved on a background curvilinear or Cartesian grids, while the complex boundaries are represented using surface meshes independent of the background grid. The effects of the boundary on the flow are modeled by reconstructing the velocity near the boundary (that the boundary conditions are not directly applied on the boundary but on grid nodes close to the boundary). In order to apply such off-wall boundary conditions, the background grid nodes are classified into fluid nodes located in the fluid, and solid nodes located in the solid. The fluid nodes near the boundary are further classified into immersed boundary (IB) nodes with neighbors in the solid and interpolation (IP) nodes close to the IB nodes. For each IB node, its velocity is reconstructed using the velocity on the boundary and IP nodes in the wall normal direction. For direct numerical simulations (DNSs), a simple linear interpolation can be employed. For wall-modeled large-eddy simulations (WMLESs), a wall model has to be employed for applying the boundary conditions at the IB nodes,[82–84] which is a challenging task for complex flows, e.g., separated flows.[85]

B. Case setup

In this work, we simulated two carotid arteries C1 and C2 from different individuals, for which the procedure for obtaining the carotid artery geometry is reported in Ref. 86. As calculated in Ref. 43, the flares of C1 and C2 are 1.51 and 2.50 and the proximal curvatures of C1 and C2 are 32.17° and 28.08°, respectively, where a flare is defined as the ratio of the maximal area of the cross section to the minimal area of the cross section with the normal of the cross sections along the axial direction of CCA before the bifurcation point and the proximal curvature measured using the angle between the axial direction of CCA and the line connecting the centroids of I2 and I3.

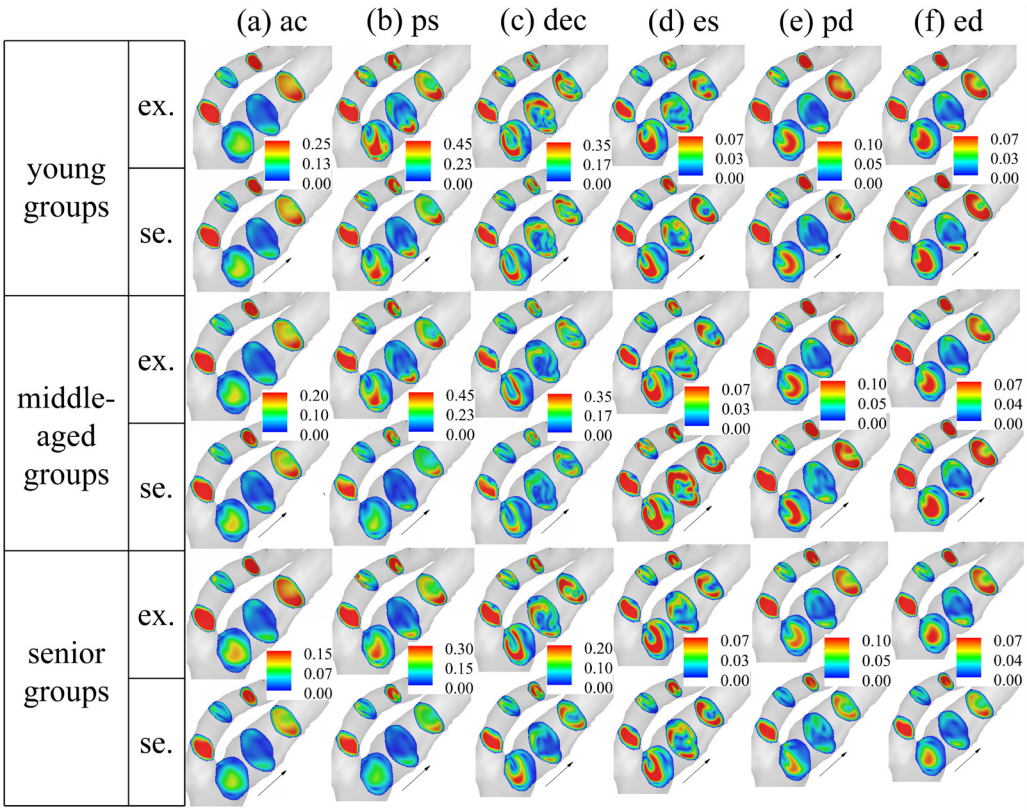

FIG. 5. Contours of velocity magnitude of the secondary flow for carotid C1 under exercise and sedentary conditions for the young, middle-aged, and senior groups, at the acceleration (a), peak systole (b), deceleration (c), end systole (d), peak diastole (e), and end diastole (f). Legend of contour: velocity magnitude of the secondary flow (m/s).

The simulation results presented by Chen *et al.*[43] showed that the reverse flow and velocity fluctuations in the carotid C2 are significantly stronger than those in C1. We will examine how different inflow waveforms affect the flow patterns in these two carotids. Due to the complexity of the carotid artery geometry, it is difficult to accurately define the range of the carotid sinus and the direction of the vessel axis at the same time. Therefore, three cross sections representing the typical positions relative to the carotid sinus, where the flow patterns are systematically examined, are manually selected. As seen in Fig. 1, I1 is located downstream of the carotid sinus (near the end of the sinus), I2 is in the middle of the carotid sinus, and I3 is upstream of the carotid sinus (near the bifurcation). The grid is uniform in all three directions with the grid spacing 0.1 mm, which is two times finer than those employed in the literature.[87] The carotid artery surface is discretized using the unstructured triangular grid (which is not shown in Fig. 1). In the simulation, the vessel wall is considered as rigid with no-slip boundary condition. The velocity at the entrance of CCA is approximated by a parabolic distribution with the flow rates given in Fig. 2. As seen, the inflow waveforms correspond to young, middle-aged, and senior persons with and without exercise (sedentary) as represented by black and red curves, respectively. As the incoming flow rate varies with time, it is convenient to use a variable time step. In this work, the Courant–Friedrichs–Lewy (CFL) number is fixed at 0.8. For all simulated cases, we simulate at least two cardiac cycles and analyze the flow field in the last cardiac cycle.

III. RESULTS

In this section, we present results from the simulated cases for the two carotids under different inflow waveforms. The analyzed characteristics of the carotid flow include the axial velocity, the secondary flow, the flow structures, the wall shear stress, the oscillatory shear index, and the statistics of the reversed flow. Six different instants, viz., the acceleration (ac), the peak of systole (ps), the deceleration (dec), the end of systole (es), the peak of diastole (pd), and the end of diastole (ed) as demonstrated in Fig. 2 are particularly analyzed.

First, we examine the axial velocity for carotid C1. In Fig. 3, we show the contours of the axial velocity of blood flow for three age groups under exercise and sedentary conditions. At the ac instant, it is observed that exercising barely affects the axial velocity for the young and middle-aged groups, while it increases the axial velocity magnitude for the senior group. At the ps instant, the blood flow velocity of the sedentary group of the same age is lower than that of the exercise group. On the other hand, at the es instant, the blood flow rate of the sedentary group of the same age group is greater than that of the exercise group for the young and middle-aged groups. Comparing the axial velocity between different age groups, it is observed that the velocity magnitude in general decreases with age at the ps instant, which can reach 1.2 m/s for the young group, drops to 1 m/s for the middle-aged group, and can only reach 0.8 m/s for the senior group. At the dec and es instants, regions with reversed flow are observed at the I2 and I3 sections located in the middle of the sinus and close to the bifurcation.

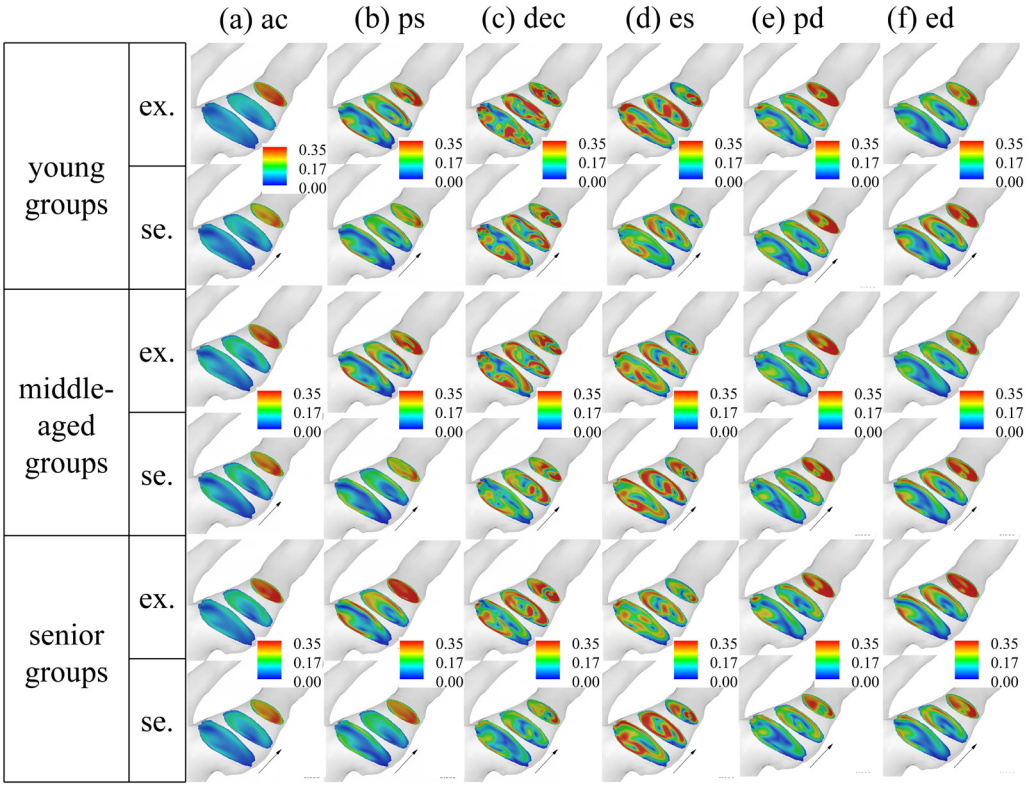

FIG. 6. Contours of velocity magnitude of the secondary flow for carotid C2 under exercise and sedentary conditions for the young, middle-aged, and senior groups, at the acceleration (a), peak systole (b), deceleration (c), end systole (d), peak diastole (e), and end diastole (f). Legend of contour: velocity magnitude of the secondary flow (m/s).

At the dec instant, it is observed that the minimal velocity of the reversed flow can reach −0.1 m/s for the young group, which is significantly less than the middle-aged and senior groups. At the pd instant, one interesting observation is that the magnitudes of the axial velocity from the middle-aged groups are slightly higher than those from the young and senior groups. Similar to those at the ac and ed instants, exercising increases the magnitude of the axial velocity for the senior groups. At the ed instant, it is observed that exercising decreases the axial velocity magnitudes for the young and middle-aged groups, which are increased for the senior group. We then examine the patterns of the axial velocity for the carotid C2. Similar trends with the carotid C1 are observed. The waveforms obtained by scrutinizing the variations among different age groups and between groups with/without exercise and the corresponding variations of the inflow are shown in Fig. 2. It can be concluded that such trends observed on the axial flow velocity are consistent with the inflow waveform. It is also observed in Figs. 3 and 4 that the overall patterns of the axial flow for different age groups with/without exercise at the same instant, with C-shaped patterns as observed in the literature,[43,48] are very similar to each other for the same carotid. However, there are some noticeable differences observed for the small-scale patterns of the axial flow especially at the dec and es instants for the carotid C2.

Here, we examine the velocity magnitude of the secondary flow for different groups. In Fig. 5, we show the computed results from the carotid C1. At the ac instant, the velocity magnitudes of the secondary flow from the exercise people and sedentary people are similar with each other for the young and middle-aged groups; for the senior group, on the other hand, the velocity magnitude of the secondary flow from the exercise people is larger than that from sedentary people. At the ps and dec instants, the velocity magnitude of the secondary flow from the exercise group is in general greater than that from the sedentary group for different ages. On the other hand, at the es instant, the velocity magnitudes of the secondary flow from the exercise group are in general lower than those from the sedentary group. At the pd instant, the velocity magnitudes of the secondary flow from the exercise and sedentary groups are similar to each other for young and middle-aged groups, while the former is slightly larger for the senior group. At the ed instant, on the other hand, exercising decreases and slightly increases the velocity magnitudes of the secondary flow for the young and middle-aged groups and the senior group, respectively. In Fig. 6, we probe into the patterns of the secondary flow for the carotid C2. Trends similar to those observed for the carotid C1 are observed for different age groups with and without exercise. One difference is that the velocity magnitude of the secondary flow is larger for people having exercised at the es instant for the carotid C2, which is not observed for the carotid C1. Generally, it is noticed that such variations in the velocity magnitudes of the secondary flow are consistent with the corresponding variations of the inflow waveform as for the axial velocity. As for the

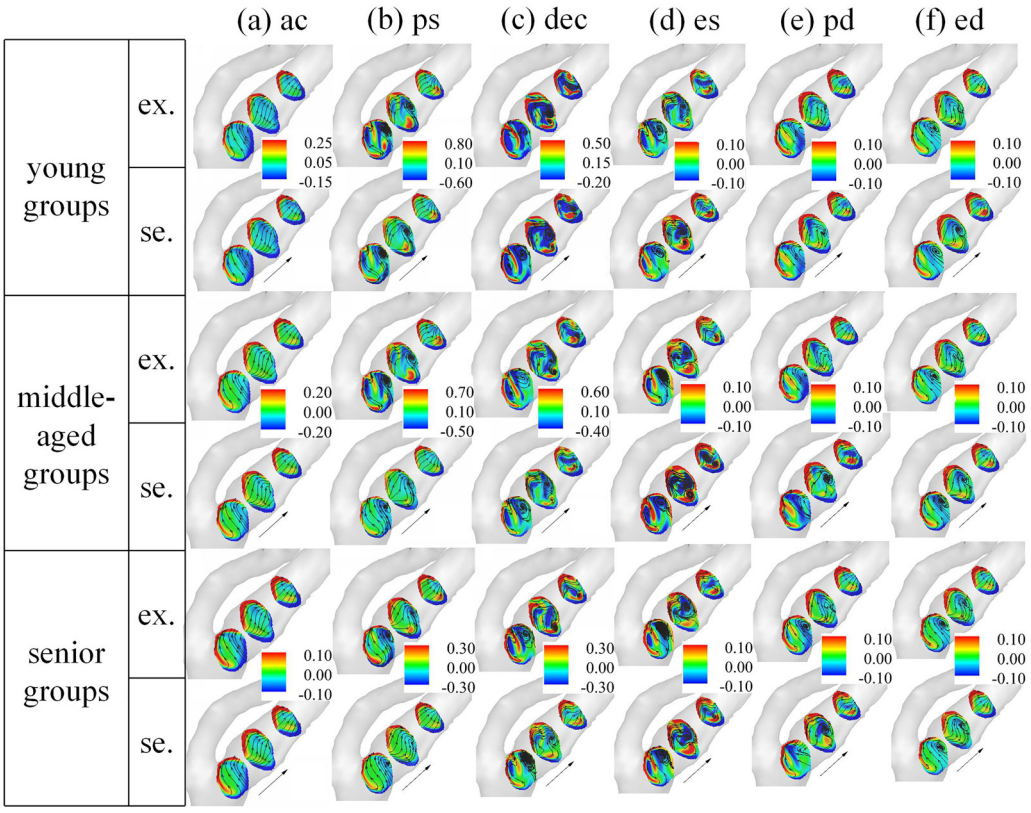

FIG. 7. Streamlines of the secondary flow on contours of the streamwise vorticity for the carotid C1 under exercise and sedentary conditions for the young, middle-aged, and senior groups, at the acceleration (a), peak systole (b), deceleration (c), end systole (d), peak diastole (e), and end diastole (f), six moments. Legend of contour: streamwise vorticity (1/s).

structures of the secondary flow, the large-scale patterns from the people having exercised, which are similar to those observed in the literature for the same carotid but under a different inflow waveform,[43] are approximately the same with sedentary people with minor differences on the small-scale patterns for the carotid C1. For the carotid C2, the comparison is complex—the overall structures are similar to each other for the exercise and sedentary groups at the ac, ps, es, pd, and ed instants, while they are different from each other at the dec instant.

Here, we examine the streamlines of the secondary flow and the streamwise vorticity. In Fig. 7, we examine the results from the carotid C1. At the ac instant, it is observed that the streamlines of the secondary flow are from one side of the blood vessel to the other with simple patterns. Regions with high vorticity magnitude of stripe-shape are located near the wall of the blood vessel on the other two sides. The vorticity magnitude decreases from young to middle-aged and senior groups. Exercising does not change the vorticity magnitude and streamlines in an obvious way. At the ps instant, the patterns of the streamlines and streamwise vorticity become complex with high magnitudes of streamwise vorticity appearing in the middle of the three cross sections. Identical to the ac instant, the vorticity magnitude decreases with age at the ps instant. Exercise increases the magnitude of the streamwise vorticity at the ps instant for different age groups. Exercise also changes the streamline pattern for the middle-aged group at this instant, which is different from the other groups. At the dec instant, the streamlines with clear dean-type vortices become more complex than those at the ps instant; that the flow structure is more complex in the deceleration phase is consistent with that reported in the literature.[43,54] Slight increases in the vorticity magnitude are observed for people having exercised for the middle-aged and senior groups. Differences between exercise and sedentary groups are observed on the small-scale patterns at I1 slices especially for the young group. At the es instant, the overall flow patterns with dean-type vortices at the I3 slices are similar to those at the dec instant, but with significantly lower vorticity magnitudes. Exercising is observed to decrease the vorticity magnitude for the middle-aged groups. The flow patterns are very close to each other for people with/without exercise for the senior group. At the pd instant, the overall flow patterns are similar to those at the es instant. The magnitudes of negative vorticity are observed to be higher in certain regions for sedentary people for the middle-aged and senior groups. At the ed instant, similar flow patterns are observed. Exercising slightly decreases the magnitudes of the negative vorticity for the young and middle-aged groups.

The results from the carotid C2 are shown in Fig. 8. The streamlines and the contours of the streamwise vorticity are simple at the ac instant, and become complex at later instants. Overall, the effects of age and exercising are similar to those for the carotid C1: (1) the vorticity magnitudes in general decrease with age at the ac, ps, and dec instants and (2) exercising increases/slightly decreases the vorticity magnitudes at certain instants for certain age groups, e.g., the ps instant for all age groups and the dec instant of the middle-aged and

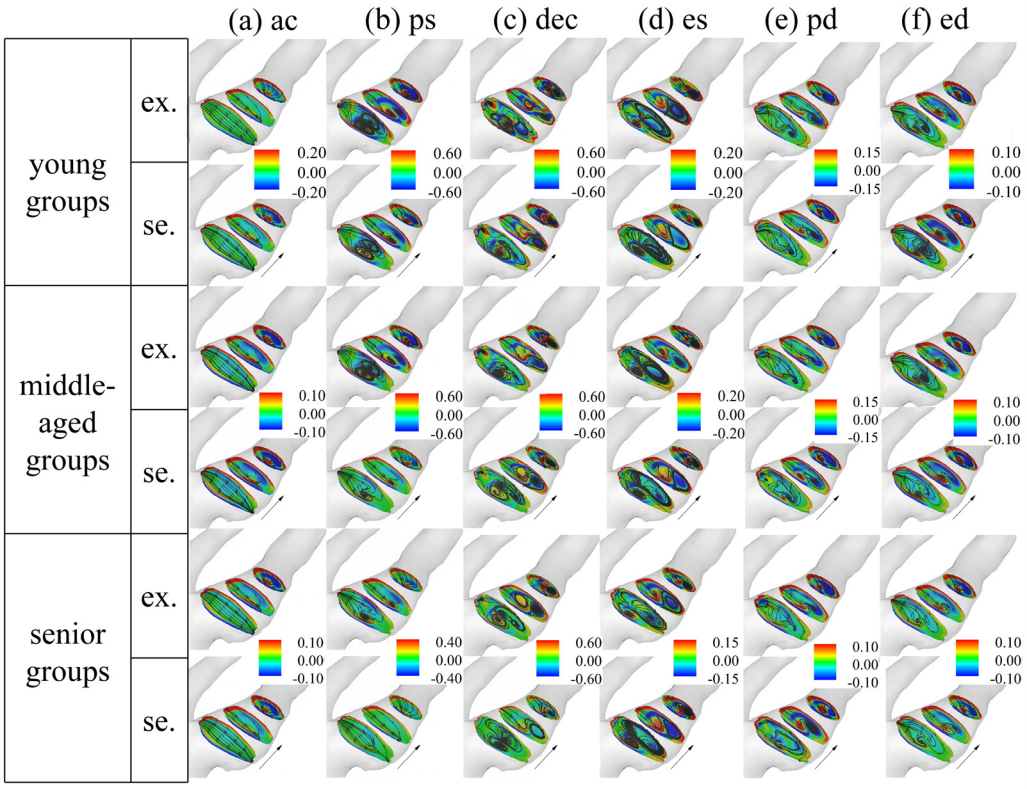

FIG. 8. Streamlines of the secondary flow on contours of the streamwise vorticity for the carotid C2 under exercise and sedentary conditions for the young, middle-aged, and senior groups, at the acceleration (a), peak systole (b), deceleration (c), end systole (d), peak diastole (e), and end diastole (f), six moments. Legend of contour: streamwise vorticity (1/s).

senior groups for those with increase effect, and the pd instant for the senior group and the ed instant for the young group for those with decreased effect. One significant difference is observed at the dec instant, at which exercising not only changes the vorticity magnitudes but also the flow structures especially for the young group.

After comparing the flow structures for different groups at the three slices, we now examine the three-dimensional flow structures identified using the Q criterion in Fig. 9 for carotid C1. It is observed that coherent flow structures start to appear at the ac instant. At the ps and dec instants, the vortex structures of the exercise group are observed to be more complicated than those of the sedentary group. Among them, at the ps instant, the elongated vortex structures of tubular shape from the exercise group are more coherent than the sedentary group. At the dec instant, the vortex structures become fairly complex for people who exercised in the young and middle-aged groups, which remain tubular shaped for the senior group. At the es instant, vortex structures of tubular shape are observed from CCA to ICA in the carotid artery. The tubular structure of the exercise group is thinner for the middle-aged and sedentary groups. At the pd instant, two long tubular-shape structures are observed for the exercise people in the middle-aged group, which are mostly connected as one for the sedentary people in the same group and the people in the young group. At the ed instant, the vortex structures from the exercise people in the young and middle-aged groups are of two long tubular-shape, which are connected for the sedentary people in the same group.

The vortex structures from the carotid C2 are shown in Fig. 10. Similar to the carotid C1, having exercised enhances the coherence of the flow structures at the ps instant for all age groups, and introduces small-scale structures at the dec instant for the young and middle-aged groups. At the pd instant, the vortex structures from the sedentary people seem to be more complex than the people having exercised. At the ed instant, the vortex structures from the people with/without having exercise are fairly similar to each other.

After showing the flow structures within the carotid, here we examine the wall shear stress of three age groups of people with/without exercise. First, we show the results from the simulation of carotid C1 in Fig. 11. At the ac instant, it is observed that the area of the brown covered surfaces located over the sinus with relatively low wall shear stress is larger for the sedentary group, and increases with age. It is also observed that the region with low wall shear stress is larger for the sedentary people when compared with people having exercised. At the ps and dec instants, the areas of the blood vessel surface with low wall shear stress (red and brown) from the exercised people and sedentary people are observed to be similar to each other for each age group. At the es instant, on the other hand, the areas with low wall shear stress are larger for people having exercised, especially for the middle-aged and senior groups. At the pd instant, the brown and red regions with low wall shear stress are approximately the same for people with/without exercise for each group, and increases with age. At the ed instant, it is observed that the red region with low wall

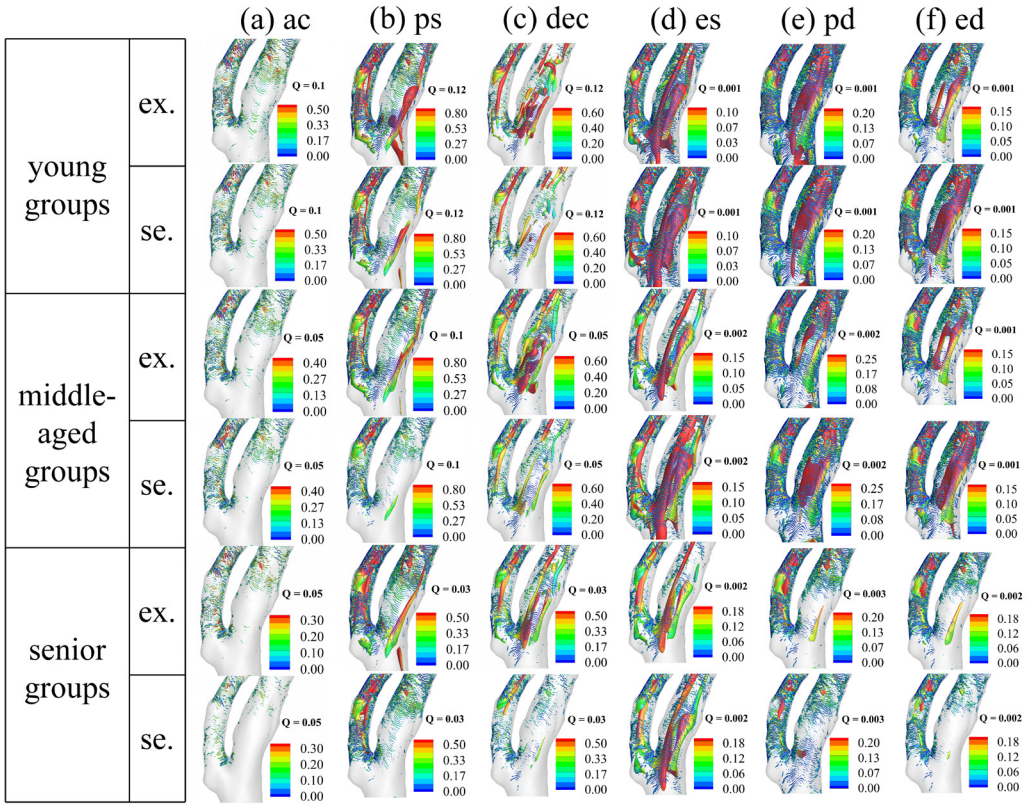

FIG. 9. Vortex structures identified using the Q criterion from the carotid C1 for young, middle-aged, and senior groups under exercise or sedentary conditions at acceleration (a), peak systole (b), deceleration (c), end systole (d), peak diastole (e), and end diastole (f). Legend of contour: velocity magnitude (m/s).

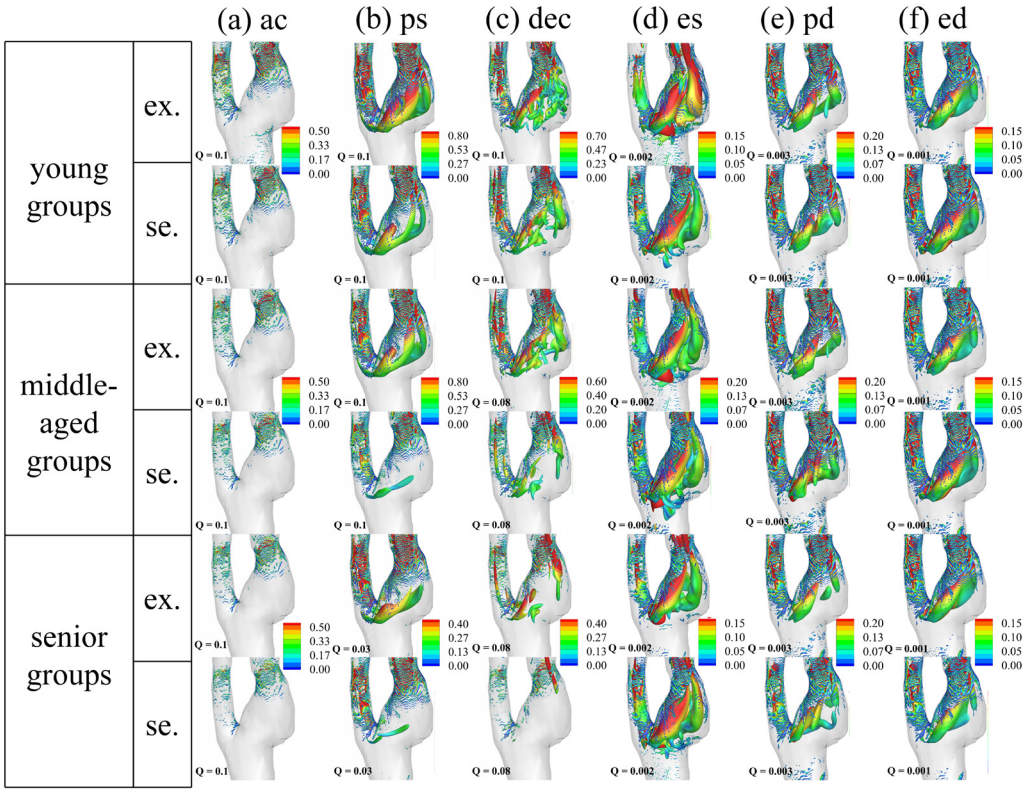

FIG. 10. The vortex structures identified using the Q criterion from the carotid C2 for young, middle-aged, and senior groups under exercise or sedentary conditions at acceleration (a), peak systole (b), deceleration (c), end systole (d), peak diastole (e), and end diastole (f). Legend of contour: velocity magnitude (m/s).

shear stress is approximately the same for different groups of different ages with/without exercise (Fig. 11).

The wall shear stresses from the carotid C2 for different groups are shown in Fig. 12. Similar to those observed on the carotid C1, the areas of the region with low wall shear stress (red) are slightly larger for the sedentary people when compared with the people having exercised at the ac instant. However, such a low wall shear stress region at the ac instant does not increase significantly with age, different from those observed on the carotid C1. At the ps instant, it is observed that exercising does not alter the area of the region with low wall shear stress for the young group, which, on the other hand, is slightly decreased (in the CCA) because of exercise for the middle-aged and senior groups. At the dec instant, the areas of the region with low wall shear stress (red) are approximately the same for different groups with/without exercise. At the es instant, exercising decreases the area with low wall shear stress (red) in the carotid sinus for the young group, which is slightly increased because of exercise for the middle-aged and senior groups. At the pd instant, the regions with low wall shear stress (red) are approximately the same with each other for groups of different ages with/without having exercise. At the ed instant, it is observed that exercising slightly increases the region with low wall shear stress (in CCA) for the young and middle-aged groups, which is decreased for the senior group.

After examining wall shear stresses at different instants, here we compare the OSI from different groups in Fig. 13, which is defined as follows:

$$\mathrm{OSI} = \left(1 - \frac{\left|\int_0^T \boldsymbol{\tau}_w dt\right|}{\int_0^T |\boldsymbol{\tau}_w| dt}\right), \tag{3}$$

where $\boldsymbol{\tau}_w$ is the wall shear stress vector and T is the period of the cardiac cycle. For carotid C1, it is observed that exercising slightly increases OSI values for different age groups. For different ages, the OSI values of the senior groups are found to be lower than those of the young and middle-aged groups. For carotid C2, the OSI values are approximately the same for groups of different ages with/without exercise.

One important flow feature observed in the carotid sinus is the reversed flow as shown in Figs. 3 and 4. Such reversed flow structures can increase the residence time of low-density lipoprotein particles in the carotid sinus, which play an important role in the formation of atherosclerosis plaques. The reversed flow ratio was examined by Chen *et al.*[43] for different carotid geometries. Here, we examine how different inflow waveforms affect the reversed flow in the carotid sinus by plotting the reversed flow volume at the three slices. The results

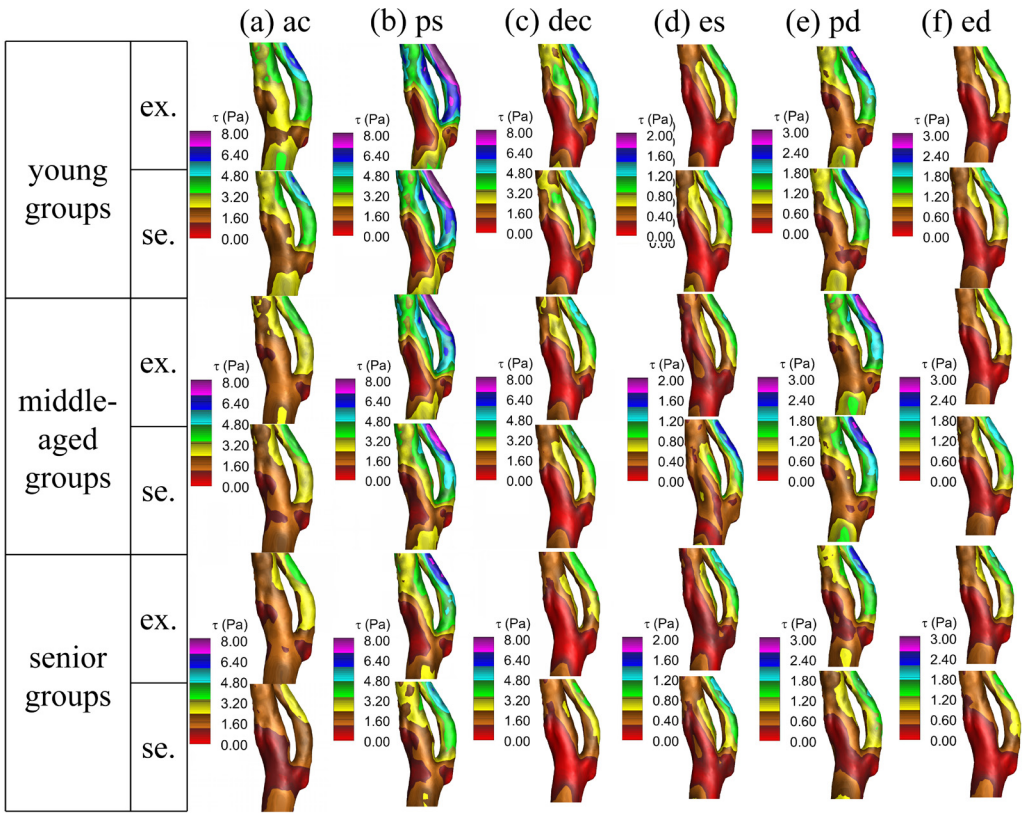

FIG. 11. Wall shear stress of the carotid artery model C1 under exercise and sedentary conditions for young, middle-aged, and senior groups at acceleration (a), peak systole (b), deceleration (c), end systole (d), peak diastole (e), and end diastole (f).

from the carotid C1 are shown in Fig. 14. As seen, on the I1 cross section, only the young group with exercise shows reversed flow at a very low flow volume at the order of 10^{-4} ml. At the I2 cross section, which is located in the middle of the carotid sinus, reversed flow volume of the order of 10^{-2} is observed. With increase in age, the reversed flow volume gradually decreases for people having exercised. For sedentary people, on the other hand, the reversed flow volumes are comparable with each other for different ages. For the young group, exercising increases the reversed flow volume from 0.0094 to 0.0165 ml. For the middle-aged group, the reversed flow volumes are approximately the same for people with/without exercise (0.0115 vs 0.0105 ml). For the senior group, on the other hand, exercising decreases the reversed flow volume from 0.008 to 0.005 ml at the I2 cross section. At the I3 cross section, which is located close to the bifurcation, the reversed flow volumes are observed to be larger than those at the I2 section. Different from I2 section, it is seen that exercising does not increase the reversed flow volume significantly (0.0136 vs 0.0125 ml) for the young group, while it decreases the reversed flow volume from 0.0177 to 0.0145 ml and the 0.0107 to 0.0071 ml, for the middle-aged and senior groups, respectively.

We then examine the reversed flow volumes for the carotid C2 as shown in Fig. 15. Similar to carotid C1, the reversed flow volumes are insignificant at the I1 section, located at the downstream end of the carotid sinus. At the other two sections, it is observed that the reversed flow volume of the carotid C2 is much greater than that of C1. When comparing the reversed flow volume at different locations, it is seen that the reversed flow volumes at the I3 section are significantly higher (∼5 times) than those at the I2 section. With age, the reversed flow volume gradually decreases for both I2 and I3 sections, which is quite different from the carotid C1, for which monotonous trends are not observed.

IV. CONCLUSIONS

Blood flow plays an important role in the formation of atherosclerosis plaques in the carotid. Many factors, such as the carotid geometry and inflow waveforms, affect the dynamics of blood flow. The carotid geometries are very different for different individuals. Previous studies have indicated that carotids with high flare and low proximal curvature are prone to atherosclerosis. The inflow waveforms change with age and are affected by exercise habits. In this work, we investigate how different inflow waveforms from people of different ages with/without exercise affect the flow patterns in two different carotids with different flares and proximal curvatures, i.e., the carotid C1 with low flare and high curvature and the carotid C2 with high flare and low curvature. The geometry of the carotid is simulated using the curvilinear immersed boundary method. The inflow waveforms from three age groups with/without exercise are examined.

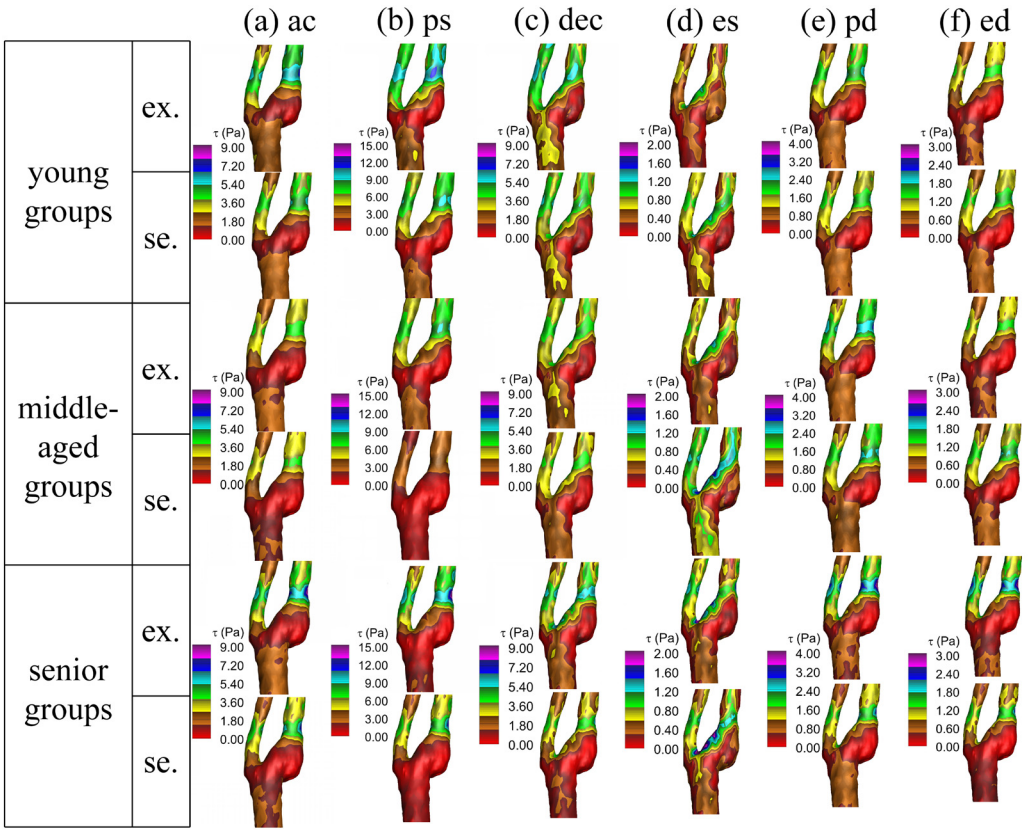

FIG. 12. Wall shear stress of the carotid artery model C2 under exercise and sedentary conditions for young, middle-aged, and senior groups at acceleration (a), peak systole (b), deceleration (c), end systole (d), peak diastole (e), and end diastole (f).

The characteristics of the flow patterns are examined. The simulation results show that the effects of inflow waveforms are different at different time instants and for different age groups. At the ps instant, exercising increases the axial velocity, the velocity magnitude of the secondary flow, and the magnitude of the streamwise vorticity for all age groups. At the dec instant, the effects of exercise on the above flow quantities are insignificant for the young groups, which, on the other hand, are enhanced for the

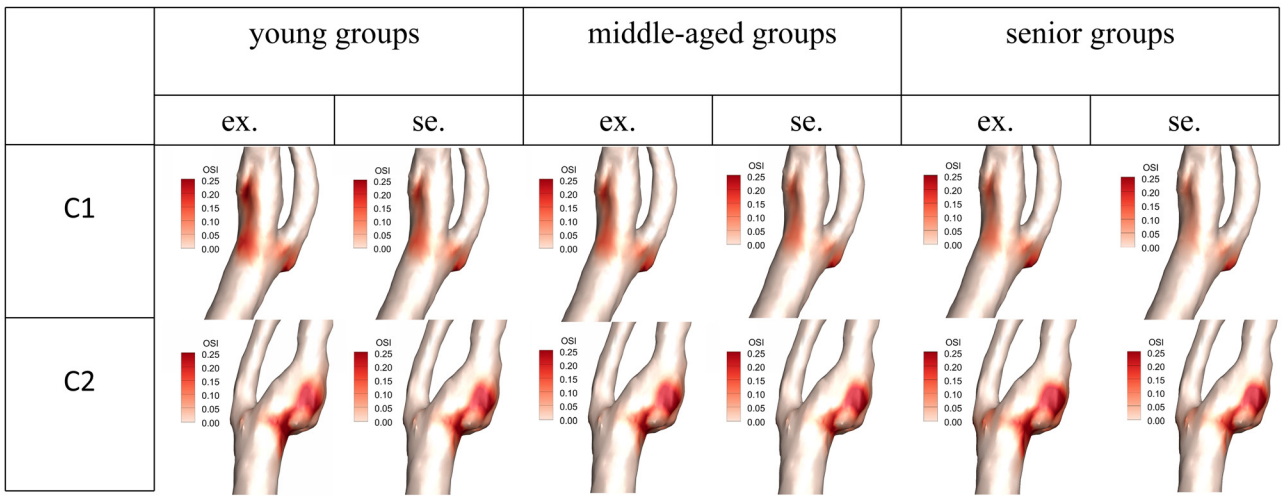

FIG. 13. Contours of oscillatory shear index (OSI) for carotids C1 and C2 for the young, middle-aged, and senior groups under exercise (ex.) or sedentary (se.) conditions.

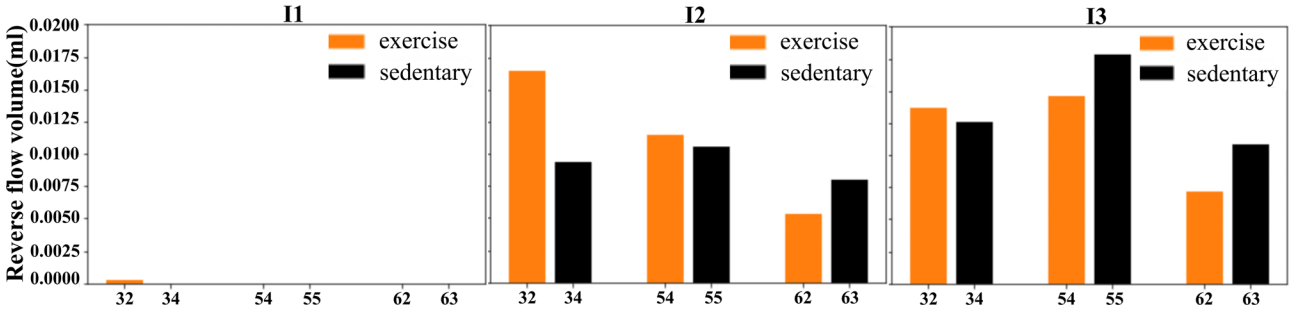

FIG. 14. Reversed flow volumes at the three slices I1, I2, and I3 for the carotid C1 for young, middle-aged, and senior groups under exercise and sedentary conditions.

senior group. At the es instant, exercising slightly decreases the magnitude of the axial velocity for the young and middle-aged groups for the carotid C1, which is insignificant for the senior group and different age groups of the carotid C2. As for the secondary flow, exercising decreases its velocity magnitude in the middle of the sinus at the es instant for the middle-aged and senior groups, which are not affected (carotid C1) or increased (carotid C2) for the young group. At the pd and ed instants, exercising increases the velocity magnitude of the axial flow and the secondary flow for the senior group, which is not observed in the young and middle-aged people. When aging, the magnitudes of the above flow quantities monotonously decrease at the ac, ps, and dec instants, which are insignificant for the other considered instants. The overall flow structures are similar to each other for different inflow waveforms for the same carotid, but show differences in the small-scale structures especially at the dec instant for young and middle-aged people for carotid C2. In general, it is observed that variations in flow characteristics are consistent with variations of the inflow waveforms. This indicates the possibility that we can reconstruct the flow structures for different inflow waveforms using the data from a baseline case.

The effects of the inflow waveforms on the wall shear stress are examined. The simulation results from the carotid C1 show that exercising decreases the area of the region with low wall shear stress at the ac instant for all age groups while increases it at the es instant for people having exercised, especially for the middle-aged and senior groups. For the carotid C2, it is observed that exercising decreases the area with low wall shear stress at the es instant for young people, while the changes are minor for other instants. For the middle-aged and senior people, the effects of exercise on the area with low wall shear stress are insignificant for all considered instants for the carotid C2. The effects of inflow waveforms on the oscillatory shear index (OSI) are examined as well. It is observed that aging gradually decreases the OSI values for the carotid C1, which, on the other hand, is insignificant for carotid C2. Exercise is observed to have very minor effects on the location and area of the region with significant OSI values. The reversed flow volumes from different age groups with/without exercise are compared as well. The simulation results from the carotid C1 show that exercising increases the reversed flow volume in the carotid sinus for the young group and decreases it for the senior group. For the middle-aged group, the reversed flow volume is slightly increased in the middle of the carotid sinus because of exercise, while it is decreased near the bifurcation location. For the carotid C2, the simulation results show that exercising increases the reversed flow volume for all ages, which gradually decreases when aging. It is also noticed that the reversed flow volume from the carotid C2 is several times larger than the carotid C1.

Overall, the effects of exercising on the dynamics of flows in human carotid are found to be different at different instants and different for different carotids. It suggests that evaluation of the effects of exercise on the initiation and formation of atherosclerosis has to be carried out considering the patient-specific geometries and their age. This work has focused on the effects of different inflow waveforms on the hemodynamics of human carotids. Further studies are needed to analyze how these flow characteristics are related to the pathogenesis of atherosclerosis. For the current findings to become helpful for the diagnosis, prevention, and surgery of atherosclerosis, the computational carotid hemodynamics has to be coupled with the physiological

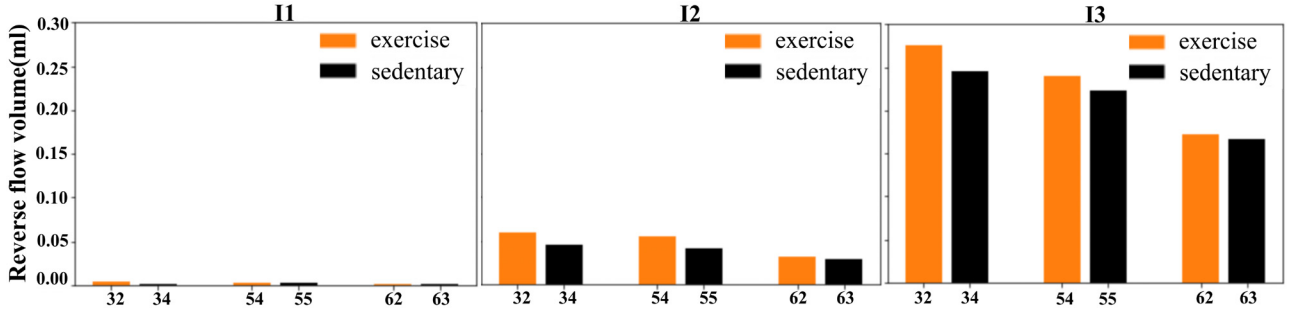

FIG. 15. Reversed flow volumes at the three slices I1, I2, and I3 for the carotid C2 for young, middle-aged, and senior groups under exercise and sedentary conditions.

and chemical process happening at the cellular scale, which will be carried out in the future work. The other limitation of the current study is the employed Newtonian fluid assumption, which will be examined in our future study.

ACKNOWLEDGMENTS

This work was partially supported by the NSFC Basic Science Center Program for "Multiscale Problems in Nonlinear Mechanics" (No. 11988102).

AUTHOR DECLARATIONS

Conflict of Interest

The authors have no conflicts to disclose.

DATA AVAILABILITY

The data that support the findings of this study are available from the corresponding author upon reasonable request.

REFERENCES

[1]F. Sotiropoulos, T. B. Le, and A. Gilmanov, "Fluid mechanics of heart valves and their replacements," Annu. Rev. Fluid Mech. **48**, 259–283 (2016).
[2]W. Choi, J. H. Park, H. Byeon, and S. J. Lee, "Flow characteristics around a deformable stenosis under pulsatile flow condition," Phys. Fluids **30**, 011902 (2018).
[3]C. Cox, M. R. Najjari, and M. W. Plesniak, "Three-dimensional vortical structures and wall shear stress in a curved artery model," Phys. Fluids **31**, 121903 (2019).
[4]T. B. Le and F. Sotiropoulos, "Fluid–structure interaction of an aortic heart valve prosthesis driven by an animated anatomic left ventricle," J. Comput. Phys. **244**, 41–62 (2013).
[5]D. N. Ku, "Blood flow in arteries," Annu. Rev. Fluid Mech. **29**, 399–434 (1997).
[6]J. M. Tarbell, Z.-D. Shi, J. Dunn, and H. Jo, "Fluid mechanics, arterial disease, and gene expression," Annu. Rev. Fluid Mech. **46**, 591–614 (2014).
[7]D. L. Fry, "Certain histological and chemical responses of the vascular interface to acutely induced mechanical stress in the aorta of the dog," Circ. Res. **24**, 93–108 (1969).
[8]A. R. Bond, S. Iftikhar, A. A. Bharath, and P. D. Weinberg, "Morphological evidence for a change in the pattern of aortic wall shear stress with age," Arterioscler., Thromb., Vasc. Biol. **31**, 543–550 (2011).
[9]M. Pikoula, "A molecular dynamics study of the vascular endothelial glycocalyx layer," Ph.D. thesis (University of Oxford, 2016).
[10]J. Tarbell and L. Cancel, "The glycocalyx and its significance in human medicine," J. Intern. Med. **280**, 97–113 (2016).
[11]A. M. W. Bartosch, R. Mathews, and J. M. Tarbell, "Endothelial glycocalyx-mediated nitric oxide production in response to selective AFM pulling," Biophys. J. **113**, 101–108 (2017).
[12]M. J. Cheng, R. Mitra, C. C. Okorafor, A. A. Nersesyan, I. C. Harding, N. N. Bal, R. Kumar, H. Jo, S. Sridhar, and E. E. Ebong, "Targeted intravenous nanoparticle delivery: Role of flow and endothelial glycocalyx integrity," Ann. Biomed. Eng. **48**, 1941 (2020).
[13]J. Albarrán-Juárez, A. Iring, S. Wang, S. Joseph, M. Grimm, B. Strilic, N. Wettschureck, T. F. Althoff, and S. Offermanns, "Piezo1 and Gq/G11 promote endothelial inflammation depending on flow pattern and integrin activation," J. Exp. Med. **215**, 2655–2672 (2018).
[14]S. Kumar, I.-H. Jang, C. W. Kim, D.-W. Kang, W. J. Lee, and H. Jo, "Functional screening of mammalian mechanosensitive genes using *Drosophila* Rnai library–Smarcd3/Bap60 is a mechanosensitive pro-inflammatory gene," Sci. Rep. **6**, 36461 (2016).
[15]X. Kong, X. Qu, B. Li, Z. Wang, Y. Chao, X. Jiang, W. Wu, and S.-L. Chen, "Modulation of low shear stress-induced eNOS multi-site phosphorylation and nitric oxide production via protein kinase and ERK1/2 signaling," Mol. Med. Rep. **15**, 908–914 (2017).
[16]J. Dunn, H. Qiu, S. Kim, D. Jjingo, R. Hoffman, C. W. Kim, I. Jang, D. J. Son, D. Kim, C. Pan *et al.*, "Flow-dependent epigenetic DNA methylation regulates endothelial gene expression and atherosclerosis," J. Clin. Invest. **124**, 3187–3199 (2014).
[17]J. Dunn, S. Thabet, and H. Jo, "Flow-dependent epigenetic DNA methylation in endothelial gene expression and atherosclerosis," Arterioscler., Thromb., Vasc. Biol. **35**, 1562–1569 (2015).
[18]J. Dunn, R. Simmons, S. Thabet, and H. Jo, "The role of epigenetics in the endothelial cell shear stress response and atherosclerosis," Int. J. Biochem. Cell Biol. **67**, 167–176 (2015).
[19]S. Kumar, D.-W. Kang, A. Rezvan, and H. Jo, "Accelerated atherosclerosis development in C_{57}Bl6 mice by overexpressing AAV-mediated PCSK9 and partial carotid ligation," Lab. Invest. **97**, 935–945 (2017).
[20]S. Kumar, C. W. Kim, R. D. Simmons, and H. Jo, "Role of flow-sensitive microRNAs in endothelial dysfunction and atherosclerosis: Mechanosensitive athero-mirs," Arterioscler., Thromb., Vasc. Biol. **34**, 2206–2216 (2014).
[21]C. Givens and E. Tzima, "Endothelial mechanosignaling: Does one sensor fit all?," Antioxid. Redox Signaling **25**, 373–388 (2016).
[22]J. Tarbell, M. Mahmoud, A. Corti, L. Cardoso, and C. Caro, "The role of oxygen transport in atherosclerosis and vascular disease," J. R. Soc. Interface **17**, 20190732 (2020).
[23]C. Karthika, S. Ahalya, N. Radhakrishnan, C. Kartha, and S. Sumi, "Hemodynamics mediated epigenetic regulators in the pathogenesis of vascular diseases," Mol. Cell. Biochem. **476**, 125–143 (2021).
[24]Y.-M. Go, C. W. Kim, D. I. Walker, D. W. Kang, S. Kumar, M. Orr, K. Uppal, A. A. Quyyumi, H. Jo, and D. P. Jones, "Disturbed flow induces systemic changes in metabolites in mouse plasma: A metabolomics study using ApoE-/- mice with partial carotid ligation," Am. J. Physiol.-Regul., Integr. Comp. Physiol. **308**, R62–R72 (2015).
[25]S. Kim, J.-H. Han, D.-H. Nam, G.-Y. Kim, J. H. Lim, J.-R. Kim, and C.-H. Woo, "PAR-1 is a novel mechano-sensor transducing laminar flow-mediated endothelial signaling," Sci. Rep. **8**, 15172 (2018).
[26]Q. Yang, J. Xu, Q. Ma, Z. Liu, V. Sudhahar, Y. Cao, L. Wang, X. Zeng, Y. Zhou, M. Zhang *et al.*, "PRKAA1/AMPKα1-driven glycolysis in endothelial cells exposed to disturbed flow protects against atherosclerosis," Nat. Commun. **9**, 4667 (2018).
[27]D. Williams, M. Mahmoud, R. Liu, A. Andueza, S. Kumar, D.-W. Kang, J. Zhang, I. Tamargo, N. Villa-Roel, K.-I. Baek *et al.*, "Stable flow-induced expression of KLK10 inhibits endothelial inflammation and atherosclerosis," BioRxiv (2021).
[28]N. Freidoonimehr, R. Chin, A. Zander, and M. Arjomandi, "Effect of shape of the stenosis on the hemodynamics of a stenosed coronary artery," Phys. Fluids **33**, 081914 (2021).
[29]M. S. Nagargoje, D. K. Mishra, and R. Gupta, "Pulsatile flow dynamics in symmetric and asymmetric bifurcating vessels," Phys. Fluids **33**, 071904 (2021).
[30]N. Freidoonimehr, R. Chin, A. Zander, and M. Arjomandi, "An experimental model for pressure drop evaluation in a stenosed coronary artery," Phys. Fluids **32**, 021901 (2020).
[31]K. Spanos, G. Petrocheilou, C. Karathanos, N. Labropoulos, D. Mikhailidis, and A. Giannoukas, "Carotid bifurcation geometry and atherosclerosis," Angiology **68**, 757–764 (2017).
[32]X. Huang, X. Yin, Y. Xu, X. Jia, J. Li, P. Niu, W. Shen, G. S. Kassab, W. Tan, and Y. Huo, "Morphometric and hemodynamic analysis of atherosclerotic progression in human carotid artery bifurcations," Am. J. Physiol.-Heart Circ. Physiol. **310**, H639–H647 (2016).
[33]A. V. Kamenskiy, I. I. Pipinos, J. S. Carson, J. N. MacTaggart, and B. T. Baxter, "Age and disease-related geometric and structural remodeling of the carotid artery," J. Vasc. Surg. **62**, 1521–1528 (2015).
[34]C. Chiastra, D. Gallo, P. Tasso, F. Iannaccone, F. Migliavacca, J. J. Wentzel, and U. Morbiducci, "Healthy and diseased coronary bifurcation geometries influence near-wall and intravascular flow: A computational exploration of the hemodynamic risk," J. Biomech. **58**, 79–88 (2017).
[35]M. Nagargoje and R. Gupta, "Effect of sinus size and position on hemodynamics during pulsatile flow in a carotid artery bifurcation," Comput. Methods Programs Biomed. **192**, 105440 (2020).

[36]K. Spanos, G. Petrocheilou, L. Livieratos, N. Labropoulos, D. P. Mikhailidis, and A. D. Giannoukas, "Carotid bifurcation geometry as assessed by ultrasound is associated with early carotid atherosclerosis," Ann. Vasc. Surg. **51**, 207–216 (2018).
[37]X. Yao, Z. Dai, X. Zhang, J. Gao, G. Xu, Y. Cai, and Z. Li, "Carotid geometry as a predictor of in-stent neointimal hyperplasia—A computational fluid dynamics study," Circ. J. **83**, 1472 (2019).
[38]H. Watase, J. Sun, D. S. Hippe, N. Balu, F. Li, X. Zhao, V. Mani, Z. A. Fayad, V. Fuster, T. S. Hatsukami *et al.*, "Carotid artery remodeling is segment specific: An *in vivo* study by vessel wall magnetic resonance imaging," Arterioscler., Thromb., Vasc. Biol. **38**, 927–934 (2018).
[39]P. Jiang, Z. Chen, D. S. Hippe, H. Watase, B. Sun, R. Lin, Z. Yang, Y. Xue, X. Zhao, and C. Yuan, "Association between carotid bifurcation geometry and atherosclerotic plaque vulnerability: A Chinese atherosclerosis risk evaluation study," Arterioscler., Thromb., Vasc. Biol. **40**, 1383–1391 (2020).
[40]S. Gregg, T. Y. Li, M.-F. Hétu, S. C. Pang, P. Ewart, and A. M. Johri, "Relationship between carotid artery atherosclerosis and bulb geometry," Int. J. Cardiovasc. Imaging **34**, 1081–1090 (2018).
[41]C. Strecker, A. J. Krafft, L. Kaufhold, M. Hüllebrandt, S. Weber, U. Ludwig, M. Wolkewitz, A. Hennemuth, J. Hennig, and A. Harloff, "Carotid geometry is an independent predictor of wall thickness—A 3D cardiovascular magnetic resonance study in patients with high cardiovascular risk," J. Cardiovasc. Magn. Reson. **22**, 67 (2020).
[42]P. B. Bijari, B. A. Wasserman, and D. A. Steinman, "Carotid bifurcation geometry is an independent predictor of early wall thickening at the carotid bulb," Stroke **45**, 473–478 (2014).
[43]Y. Chen, X. Yang, A. J. Iskander, and P. Wang, "On the flow characteristics in different carotid arteries," Phys. Fluids **32**, 101902 (2020).
[44]A. Azhim, M. Katai, M. Akutagawa, Y. Hirao, K. Yoshizaki, S. Obara, M. Nomura, H. Tanaka, H. Yamaguchi, and Y. Kinouchi, "Blood flow velocities in common carotid artery changes with age and exercise study by using of telemetry method," in *International Conference on Biomedical and Pharmaceutical Engineering* (IEEE, 2006), pp. 523–530.
[45]R. Rauramaa, P. Halonen, S. B. Väisänen, T. A. Lakka, A. Schmidt-Trucksäss, A. Berg, I. M. Penttilä, T. Rankinen, and C. Bouchard, "Effects of aerobic physical exercise on inflammation and atherosclerosis in men: The DNASCO study: A six-year randomized, controlled trial," Ann. Intern. Med. **140**, 1007–1014 (2004).
[46]N. Kadoglou, F. Iliadis, and C. Liapis, "Exercise and carotid atherosclerosis," Eur. J. Vasc. Endovasc. Surg. **35**, 264–272 (2008).
[47]Q. Huang, J. Sun, and C. Xu, "Effects of waveform shape of pulsatile blood flow on hemodynamics in an artery bifurcation model," Proc. Inst. Mech. Eng., Part C **235**, 428–440 (2021).
[48]C. Rindt *et al.*, "Unsteady flow in a rigid 3D model of the carotid artery bifurcation," J. Biomech. Eng. **118**, 90–96 (1996).
[49]M. W. Plesniak and K. V. Bulusu, "Morphology of secondary flows in a curved pipe with pulsatile inflow," J. Fluids Eng. **138**, 101203 (2016).
[50]M. R. Najjari and M. W. Plesniak, "Evolution of vortical structures in a curved artery model with non-Newtonian blood-analog fluid under pulsatile inflow conditions," Exp. Fluids **57**, 100 (2016).
[51]M. R. Najjari and M. W. Plesniak, "Secondary flow vortical structures in a 180° elastic curved vessel with torsion under steady and pulsatile inflow conditions," Phys. Rev. Fluids **3**, 013101 (2018).
[52]F. Ahmed, I. Eames, E. Moeendarbary, and A. Azarbadegan, "High-Strouhal-number pulsatile flow in a curved pipe," J. Fluid Mech. **923**, A15 (2021).
[53]N. A. Buchmann and M. C. Jermy, "Blood flow measurements in idealised and patient specific models of the human carotid artery," in *Proceedings of the 14th International Symposium on Applications of Laser Techniques to Fluid Mechanics* (Citeseer, 2008), pp. 7–10.
[54]Y. A. Gataulin, D. K. Zaitsev, E. M. Smirnov, and A. D. Yukhnev, "Numerical study of spatial-temporal evolution of the secondary flow in the models of a common carotid artery," St. Petersburg Polytech. Univ. J. **3**, 1–6 (2017).
[55]M. Sakthivel and K. Anupindi, "An off-lattice Boltzmann method for blood flow simulation through a model irregular arterial stenosis: The effects of amplitude and frequency of the irregularity," Phys. Fluids **33**, 031912 (2021).
[56]V. Carvalho, N. Rodrigues, R. Ribeiro, P. F. Costa, J. C. Teixeira, R. A. Lima, and S. F. Teixeira, "Hemodynamic study in 3D printed stenotic coronary artery models: Experimental validation and transient simulation," Comput. Methods Biomech. Biomed. Eng. **24**, 623–614 (2021).
[57]J. Song, S. Kouidri, and F. Bakir, "Numerical study on flow topology and hemodynamics in tortuous coronary artery with symmetrical and asymmetrical stenosis," Biocybern. Biomed. Eng. **41**, 142–155 (2021).
[58]G. Ding, K.-S. Choi, B. Ma, T. Kato, and W. Yuan, "Transitional pulsatile flows with stenosis in a two-dimensional channel," Phys. Fluids **33**, 034115 (2021).
[59]C. Cox and M. W. Plesniak, "The effect of entrance flow development on vortex formation and wall shear stress in a curved artery model," Phys. Fluids **33**, 101908 (2021).
[60]W. Choi, H. M. Kim, S. Park, E. Yeom, J. Doh, and S. J. Lee, "Variation in wall shear stress in channel networks of zebrafish models," J. R. Soc. Interface **14**, 20160900 (2017).
[61]S. Kumar, C. W. Kim, D. J. Son, C. W. Ni, and H. Jo, "Flow-dependent regulation of genome-wide mRNA and microRNA expression in endothelial cells *in vivo*," Sci. Data **1**, 140039 (2014).
[62]K. Vahidkhah, *Three-Dimensional Computational Simulation of Multiscale Multiphysics Cellular/Particulate Processes in Microcirculatory Blood Flow* (Rutgers The State University of New Jersey-New Brunswick, 2015).
[63]A. G. Hoekstra, S. Alowayyed, E. Lorenz, N. Melnikova, L. Mountrakis, B. Van Rooij, A. Svitenkov, G. Závodszky, and P. Zun, "Towards the virtual artery: A multiscale model for vascular physiology at the physics–chemistry–biology interface," Philos. Trans. R. Soc. A **374**, 20160146 (2016).
[64]A. Sakellarios, C. V. Bourantas, S.-L. Papadopoulou, Z. Tsirka, T. de Vries, P. H. Kitslaar, C. Girasis, K. K. Naka, D. I. Fotiadis, S. Veldhof *et al.*, "Prediction of atherosclerotic disease progression using LDL transport modelling: A serial computed tomographic coronary angiographic study," Eur. Heart J.-Cardiovasc. Imaging **18**, 11–18 (2017).
[65]F. Donadoni, C. Pichardo-Almarza, M. Bartlett, A. Dardik, S. Homer-Vanniasinkam, and V. Díaz-Zuccarini, "Patient-specific, multi-scale modeling of neointimal hyperplasia in vein grafts," Front. Physiol. **8**, 226 (2017).
[66]A. N. Beris, J. S. Horner, S. Jariwala, M. Armstrong, and N. J. Wagner, "Recent advances in blood rheology: A review," Soft Matter **17**, 10591 (2021).
[67]K. Giannokostas, P. Moschopoulos, S. Varchanis, Y. Dimakopoulos, and J. Tsamopoulos, "Advanced constitutive modeling of the thixotropic elasto-visco-plastic behavior of blood: Description of the model and rheological predictions," Materials **13**, 4184 (2020).
[68]A. J. Apostolidis and A. N. Beris, "The effect of cholesterol and triglycerides on the steady state shear rheology of blood," Rheol. Acta **55**, 497–509 (2016).
[69]K. Giannokostas, D. Photeinos, Y. Dimakopoulos, and J. Tsamopoulos, "Quantifying the non-Newtonian effects of pulsatile hemodynamics in tubes," J. Non-Newtonian Fluid Mech. **298**, 104673 (2021).
[70]S. Kang, A. Lightbody, C. Hill, and F. Sotiropoulos, "High-resolution numerical simulation of turbulence in natural waterways," Adv. Water Resour. **34**, 98–113 (2011).
[71]X. Yang, F. Sotiropoulos, R. J. Conzemius, J. N. Wachtler, and M. B. Strong, "Large-eddy simulation of turbulent flow past wind turbines/farms: The virtual wind simulator (VWiS)," Wind Energy **18**, 2025–2045 (2015).
[72]A. Calderer, X. Yang, D. Angelidis, A. Khosronejad, T. Le, S. Kang, A. Gilmanov, L. Ge, and I. Borazjani, "Virtual flow simulator," Report No. 004806MLTPL00 (University of Minnesota, 2015).
[73]X. Yang, D. Angelidis, A. Khosronejad, T. Le, S. Kang, A. Gilmanov, L. Ge, I. Borazjani, and A. Calderer, "Virtual flow simulator [computer software]," USDOE Office of Energy Efficiency and Renewable Energy (EERE), https://github.com/SAFL-CFD-Lab/VFS-Wind.
[74]S. Li, X. Yang, G. Jin, and G. He, "Wall-resolved large-eddy simulation of turbulent channel flows with rough walls," Theor. Appl. Mech. Lett. **11**, 100228 (2021).
[75]Z. Li and X. Yang, "Large-eddy simulation on the similarity between wakes of wind turbines with different yaw angles," J. Fluid Mech. **921**, A11 (2021).
[76]Z. Zhou, T. Wu, and X. Yang, "Reynolds number effect on statistics of turbulent flows over periodic hills," Phys. Fluids **33**, 105124 (2021).
[77]L. Ge and F. Sotiropoulos, "A numerical method for solving the 3D unsteady incompressible Navier-Stokes equations in curvilinear domains with complex immersed boundaries," J. Comput. Phys. **225**, 1782–1809 (2007).
[78]A. Gilmanov and F. Sotiropoulos, "A hybrid cartesian/immersed boundary method for simulating flows with 3D, geometrically complex, moving bodies," J. Comput. Phys. **207**, 457–492 (2005).

[79]I. Borazjani, L. Ge, and F. Sotiropoulos, "Curvilinear immersed boundary method for simulating fluid structure interaction with complex 3D rigid bodies," J. Comput. Phys. **227**, 7587–7620 (2008).
[80]A. Khosronejad, S. Kang, I. Borazjani, and F. Sotiropoulos, "Curvilinear immersed boundary method for simulating coupled flow and bed morphodynamic interactions due to sediment transport phenomena," Adv. Water Resour. **34**, 829–843 (2011).
[81]A. Gilmanov, T. B. Le, and F. Sotiropoulos, "A numerical approach for simulating fluid structure interaction of flexible thin shells undergoing arbitrarily large deformations in complex domains," J. Comput. Phys. **300**, 814–843 (2015).
[82]X. Yang, G.-W. He, and X. Zhang, "Towards large-eddy simulation of turbulent flows with complex geometric boundaries using immersed boundary method," AIAA Paper No. AIAA-2010-708, 2010.
[83]S. Kang, "An improved near-wall modeling for large-eddy simulation using immersed boundary methods," Int. J. Numer. Methods Fluids **78**, 76–88 (2015).
[84]B. Shi, X. Yang, G. Jin, G. He, and S. Wang, "Wall-modeling for large-eddy simulation of flows around an axisymmetric body using the diffuse-interface immersed boundary method," Appl. Math. Mech. **40**, 305–320 (2019).
[85]Z. Zhou, G. He, and X. Yang, "Wall model based on neural networks for les of turbulent flows over periodic hills," Phys. Rev. Fluids **6**, 054610 (2021).
[86]A. J. Iskander, R. Naftalovich, and X. Yang, "The carotid sinus acts as a mechanotransducer of shear oscillation rather than a baroreceptor," Med. Hypotheses **134**, 109441 (2020).
[87]K. Moyle, G. Mallinson, C. Occleshaw, B. Cowan, and T. Gentles, "Wall shear stress is the primary mechanism of energy loss in the fontan connection," Pediatr. Cardiol. **27**, 309–315 (2006).